Solving hydro-mechanical problems with the material point method

A. Yerro Colom[1]
Universitat Politecnica de Catalunya, Barcelona, Spain

ABSTRACT

This paper presents the ongoing work aimed at developing the material point method (MPM) to solve geomechanical problems. Although MPM is usually classified as a mesh-free method, it might rather be classified as a method in between the well-known finite element method (FEM) and true particle-based methods. MPM uses two different discretizations. One is the Lagrangian discretization and the other one is the Eulerian mesh. The advantages of both frames are exploited by mapping the appropriate data between them. The problem of mesh distortion, found with the Lagrangian FEM is eliminated. MPM proved to be a powerful tool for the simulation of large deformation problems, especially those involving complex geometries and contact boundaries. An important issue of this work is the coupling of hydraulic and mechanical aspects. Results in the context of a few idealized geotechnical problems are presented in this work in order to test the presented formulation.

Keywords: material point method, finite elements, mesh-free method, Eulerian-Lagrangian formulation.

1 INTRODUCTION

Problems involving large deformations such as dynamic evolution of landslides or problems involving history-dependent constitutive models are of great interest in the geotechnical field. The study of these problems in solid mechanics often implies a good understanding of dynamic behavior of saturated porous media.

The material point method (MPM; Sulsky et al. [1], [2]; Sulsky & Schreyer [3]) still resembles classical FEM in many respects. Much of the knowledge and research in FEM can be transferred to MPM. The latter uses two different discretization strategies: the material or Lagrangian mesh represented by the material points and the spatial or Eulerian mesh defined over the computational domain. Each material point carries all the information meanwhile the governing equations are solved on the Eulerian grid.

In the past decade, some geotechnical problems have been solved using MPM, such as the studies developed by Bardenhagen et al. [4] proposing a model for granular materials and Coetzee and Vermeer [5] modeling anchors placed in soil. In most of them, the media is considered as a single-phase material. In other recent works the interaction between different phases has been taken into account such as the numerical study of D.Z. Shang et al. [7] and the work of F. Zabala & E.E. Alonso [6] analyzing the Aznalcóllar progressive failure in Spain.

In this work the solid skeleton and pore fluid interaction has been taken into account. The

[1] Dep of Geotechnical Eng and Geo-Sciences (ETCG), Universitat Politecnica de Catalunya , c/ Jordi Girona 1-3, Campus Nort, Edifici D-2, 08034 Barcelona, Spain. alba.yerro@upc.edu

displacements - pore pressure formulation (*u-p*) developed by Zienkiewicz et al. [8] has been used to predict the dynamic behavior of saturated porous media.

2 GOVERNING EQUATIONS

The governing equations of saturated media, considering the dynamic problem, are the standard momentum conservation and the mass balance equation. These can be written as

$$\rho\ddot{\mathbf{u}} = \nabla\cdot\boldsymbol{\sigma} + \rho\mathbf{b} \tag{1}$$

$$\nabla\cdot\dot{\mathbf{u}} + \left(\frac{(1-n)}{\mathrm{K}_s} + \frac{n}{\mathrm{K}_f}\right)\dot{p} + \nabla\cdot\mathbf{w} = 0 \tag{2}$$

in which $\mathbf{u}$ is the solid displacement, $\dot{\mathbf{u}}$ is the solid velocity and $\ddot{\mathbf{u}}$ is the solid acceleration; p is the pore pressure and $\dot{p}$ is the pressure increment; n is the porosity, K_s and K_f are the bulk modulus of solid skeleton and pore fluid and $\mathbf{b}$ are the body forces. The density of the mixture is

$$\rho = (1-n)\rho_s + n\rho_f \tag{3}$$

where ρ_s and ρ_f are the densities of the solid and fluid phases. The Cauchy stress tensor is represented by

$$\boldsymbol{\sigma} = \boldsymbol{\sigma}' - p\mathbf{I} \tag{4}$$

in which $\boldsymbol{\sigma}'$ is the effective stress tensor and $\mathbf{I}$ is the identity matrix. Finally the relative fluid Darcy velocity is expressed by

$$\mathbf{w} = -\frac{\mathbf{k}}{\rho_f g}\cdot\left(\nabla p - \rho_f\mathbf{b} + \rho_f\ddot{\mathbf{u}}\right) \tag{5}$$

where $\mathbf{k}$ is the permeability tensor, ∇p is the pressure gradient and g is the gravity.

The initial conditions for the dynamic analysis are written as

$$\mathbf{u} = \mathbf{u}_0 \quad , \quad \dot{\mathbf{u}} = \dot{\mathbf{u}}_0 \quad , \quad p = p_0 \,. \tag{6}$$

The mechanical boundary conditions are given by

$$\mathbf{u}(\mathbf{x},t) = \bar{\mathbf{u}}(t) \qquad \text{on} \quad \partial\Omega^u \tag{7}$$

$$\boldsymbol{\sigma}(\mathbf{x},t)\cdot\mathbf{n} = \bar{\mathbf{t}}(t) \quad \text{on} \quad \partial\Omega^t \tag{8}$$

in which $\partial\Omega^u$ is the boundary where the displacement prescribed and $\partial\Omega^t$ is the boundary where the prescribed traction is applied.

The hydraulic boundary conditions are expressed by

$$p(\mathbf{x},t) = \bar{p}(t) \qquad \text{on} \quad \partial\Omega^p \tag{9}$$

$$\mathbf{w}(\mathbf{x},t)\cdot\mathbf{n} = \bar{w}(t) \quad \text{on} \quad \partial\Omega^w \tag{10}$$

in which $\partial\Omega^p$ is the boundary where the pore pressure is prescribed and $\partial\Omega^w$ is the boundary where the external fluid flux is applied.

3 MPM FOR SATURATED PORUS MEDIA

3.1 Weak form of the governing equations

The Galerkin method of Weighted Residuals has been applied in order to obtain the weak form of the governing equations over the domain Ω. The weak form for the Eq. (1) can be expressed as

$$\begin{aligned}&\int_\Omega \delta\mathbf{u}\cdot\rho\ddot{\mathbf{u}}d\Omega = \int_{\partial\Omega^t}\delta\mathbf{u}\cdot\bar{\mathbf{t}}d\Omega^t \\ &-\int_\Omega \nabla\delta\mathbf{u}:\boldsymbol{\sigma}d\Omega + \int_\Omega \delta\mathbf{u}\cdot\rho\mathbf{b}d\Omega\end{aligned} \,. \tag{11}$$

Here $\delta\mathbf{u}$ denotes the test function for the mechanical problem. The weak form for the Eq. (2) can be written as

$$\begin{aligned}&\int_\Omega \delta p Q\dot{p}d\Omega = -\int_\Omega \delta p(\nabla\cdot\dot{\mathbf{u}})d\Omega \\ &-\int_{\partial\Omega^w}\delta p\bar{w}d\partial\Omega + \int_\Omega(\nabla\delta p)\cdot\mathbf{w}d\Omega\end{aligned} \,. \tag{12}$$

Here δp designates the test function for the hydraulic problem. Q is a coefficient which has the following expression.

$$Q = \frac{(1-n)}{\mathrm{K_s}} + \frac{n}{\mathrm{K}_f} \tag{13}$$

3.2 Space discretization

MPM dicretizes the media in two different frames: Lagrangian and Eulerian (Figure 1).

In the first one, the continuum is divided into a finite number of subdomains called material points or particles (Figure 1). Each material point moves attached with the solid skeleton, carrying all the information (displacement, velocity, pore pressure, etc.). These provide the Lagrangian description of the media. Assuming that the whole mass of a material point is concentrated at the corresponding material point, the density of the mixture can be expressed as

$$\rho(\mathbf{x},t) = \sum_{p=1}^{N_p} m_p \delta(\mathbf{x} - \mathbf{x}_p) \tag{14}$$

in which m_p and $\mathbf{x}_p$ are the mass and the position of the p_{th} material point, $\delta(\mathbf{x})$ is the Dirac delta function, and N_p is the total number of particles.

In the second one, the Eulerian computational mesh is the same as the one used in the conventional FEM (Figure 1). The standard shape functions $\mathbf{N}_j$ for the discretization of $\mathbf{u}$ and N_j for the discretization of p will provide us the relationship between the nodes and any point of the domain. The displacements and the pore pressure of any material point are represented, respectively, by

$$\mathbf{u}_p = \sum_{j=1}^{Nn} \mathbf{u}_j \cdot \mathbf{N}_j^p \tag{15}$$

$$p_p = \sum_{j=1}^{Nn} p_j N_j^p \,. \tag{16}$$

Here $\mathbf{u}_j$ and p_j are the displacement and the pore pressure of the j_{th} node of the mesh and N_n is the total number of nodes.

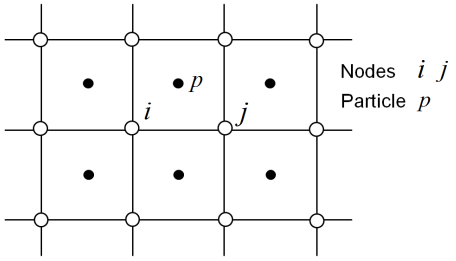

Figure 1. Space discretization - nodes of the computational mesh and particles.

The final discrete forms for the Eqs. (11) and (12) applying the spatial discretizations yield

$$\begin{aligned}
&\sum_{p=1}^{Np} m_p \mathbf{N}_i^p \cdot \mathbf{N}_j^p \cdot \ddot{\mathbf{u}}_j \\
&+\sum_{p=1}^{Np} \nabla \mathbf{N}_i^p \cdot \mathbf{D} \cdot \nabla \mathbf{N}_j^p V_p \cdot \mathbf{u}_j \\
&+\sum_{p=1}^{Np} \tilde{N}_i^p \boldsymbol{\alpha} \cdot \nabla \mathbf{N}_j^p V_p \quad p_j \\
&= \int_{\partial\Omega^t} \mathbf{N}_i^p \cdot \bar{\mathbf{t}} d\Omega \Big|_{\mathbf{x}=\mathbf{x}_p} + \sum_{p=1}^{Np} m_p \mathbf{N}_i^p \cdot \mathbf{b}
\end{aligned} \tag{17}$$

$$\begin{aligned}
&\sum_{p=1}^{Np} \tilde{N}_i^p Q \tilde{N}_j^p V_p \dot{p}_j \\
&+\sum_{p=1}^{Np} \nabla \tilde{N}_i^p \cdot \frac{\mathbf{k}}{\rho_f g} \cdot \nabla \tilde{N}_j^p V_p p_j \\
&+\sum_{p=1}^{Np} \tilde{N}_i^p \boldsymbol{\alpha} \cdot \nabla \mathbf{N}_j^p V_p \cdot \dot{\mathbf{u}}_j \\
&= \sum_{p=1}^{Np} \nabla \tilde{N}_i^p \cdot \frac{\mathbf{k}}{g} \cdot \mathbf{b} V_p - \int_{\partial\Omega^w} \tilde{N}_i^p \bar{w} d\partial\Omega^w \Big|_{\mathbf{x}=\mathbf{x}_p}
\end{aligned} \tag{18}$$

where $\mathbf{D}$ is the matrix of the constitutive model considered, the vector $\boldsymbol{\alpha} = (1\ 1\ 1\ 0\ 0\ 0)$ and V_p is the volume associated with each material point.

Eqs. (17) and (18) can be written as follows:

$$\ddot{\mathbf{u}}_j = \frac{1}{\mathbf{m}_{ij}} \cdot \left(\mathbf{f}_i^{\mathbf{u}} - \mathbf{k}_{ij} \cdot \mathbf{u}_j - \mathbf{r}_{ij}^{\mathrm{T}} p_j \right) \tag{19}$$

$$\dot{p}_j = \frac{1}{s_{ij}} \left(f_i^p - h_{ij} p_j - \mathbf{r}_{ij} \cdot \dot{\mathbf{u}}_j \right). \tag{20}$$

3.3 Time integration

In this work the explicit Euler scheme has been used for the time discretization. The acceleration and the increment of the pore pressure at nodes are the unknowns of the system of equations. The updated displacement, velocity and pore pressure at particle can be calculated as

$$\mathbf{u}_p^{\,t+\Delta t} = \mathbf{u}_p^{\,t} + \Delta t \dot{\mathbf{u}}_p^{\,t} \tag{21}$$

$$\dot{\mathbf{u}}_p^{\,t+\Delta t} = \dot{\mathbf{u}}_p^{\,t} + \Delta t \ddot{\mathbf{u}}_p^{\,t} \tag{22}$$

$$p_p^{\,t+\Delta t} = p_p^{\,t} + \Delta t \dot{p}_p^{\,t}. \tag{23}$$

where t is the current time and Δt the time step.

3.4 Algorithm

In order to avoid numerical problems the momentum at nodes instead of acceleration has been used to solve the system. This procedure was proposed to solve mechanical problems with MPM by Sulsky et al. [2], and it was improved by Wiezckowski [9]. Then, the order of the steps in each computational cycle is as follows

- Apply the initial conditions to the particles.
- Calculate the nodal velocities solving the following system of equations.

$$\mathbf{m}_i^t \cdot \dot{\mathbf{u}}_i^t = \sum_{p=1}^{Np} m_p^t \mathbf{N}_i^t \cdot \dot{\mathbf{u}}_p^t \tag{24}$$

- Calculate the total vector of nodal forces.

$$\mathbf{f}_i^t = \mathbf{f}_i^{\mathbf{u},t} - \mathbf{k}_{ij}^t \cdot \mathbf{u}_j^t - \mathbf{r}_{ij}^{t\,\mathbf{T}} p_j^t \tag{25}$$

- Calculate the nodal accelerations by solving Eq. (19).
- Update the material point velocities according to Eq. (22).
- Update the nodal velocities solving the following system of equations,

$$\mathbf{m}_i^t \cdot \dot{\mathbf{u}}_i^{t+\Delta t} = \sum_{p=1}^{Np} m_p^t \mathbf{N}_i^t \cdot \dot{\mathbf{u}}_p^{t+\Delta t}. \tag{26}$$

- Evaluate the strain increment at each material point using the nodal updated velocities. Small deformations are assumed.

$$\dot{\boldsymbol{\varepsilon}}_p^t = \frac{1}{2} \sum_{i=1}^{N_n} \left(\dot{\mathbf{u}}_i^{t+dt} \nabla \mathbf{N}_i^p + \dot{\mathbf{u}}_i^{t+dt} \left(\nabla \mathbf{N}_i^p \right)^{\mathbf{T}} \right) \tag{27}$$

- Update stress and calculate the strain on the material points using the appropriate constitutive model.

$$\boldsymbol{\varepsilon}_p^{t+dt} = \boldsymbol{\varepsilon}_p^t + \Delta t \dot{\boldsymbol{\varepsilon}}_p^t \tag{28}$$

$$\boldsymbol{\sigma}_p^{t+dt} = \mathbf{D} : \boldsymbol{\varepsilon}_p^{t+dt} \tag{29}$$

- Update the displacement of the material points according to Eq. (21).
- Calculate the vector of nodal pore pressure increments solving Eq. (20).
- Update the pore pressure at the material points according to Eq. (23).
- Update the rest of state variables (density, porosity, particle mass, Darcy velocity).
- Updated time for the next time increment and discard the information associated with the computational mesh.

A computational code is being developed to solve hydro-mechanical problems using MPM.

4 NUMERICAL EXAMPLES

This section aims to test the code reproducing two simple problems: the vibration of an elastic beam and a flow problem in a saturated porous medium. Both models are analyzed as 1-D problem. Linear shape functions and 2-node elements have been used.

4.1 *Vibration of a continuum beam*

The first analyzed problem is a simple mechanical problem of vibration of a continuum beam. This has been discussed by Bardenhagen in [10] The Young's modulus adopted is $E = 10\,\text{Pa}$, the density of the material is $\rho = 1\,\text{kg/m}$ and the length is $L = 1\,\text{m}$. The number of particles considered in the example is $Np = 13$ and the number of nodes of the computational mesh is $Nn = 14$ (Figure 2).

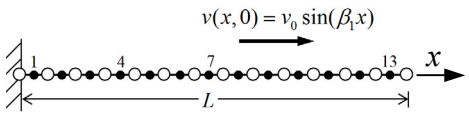

Figure 2. Continuum bar vibration problem. The bar is represented by 13 material points.

For this example, only the first vibration mode has been considered. The analytical solution for the displacements is

$$u(x,t) = \frac{v_0}{\omega_1}\sin(\omega_1 t)\sin(\beta_1 t)\cdot \tag{30}$$

where $v_0 = 0.1\,\text{m/s}$, $\omega_1 = \frac{\pi}{2L}\sqrt{\frac{E}{\rho}}$ and $\beta_1 = \frac{\pi}{2L}$.

Numerical and analytical results are compared in Figure 3.

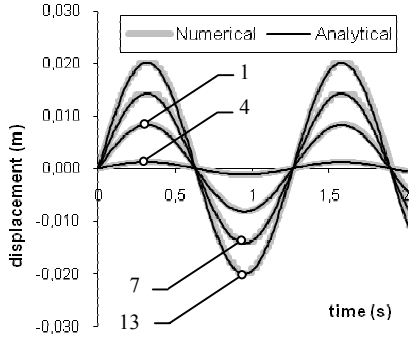

Figure 3. Numerical and analytical results for particles 1, 4, 7 and 13 of a continuum bar.

As shown in the figure the numerical results reproduce the analytical solution. Amplitude of particle displacements increase as the distance of the fixed boundary increases.

4.2 *Darcy's flow*

The second case is a hydrological problem in which a saturated soil sample is considered. The initial pore pressure in the sample is zero. A pressure of 100 Pa is prescribed in one boundary whereas in the opposite one the pressure is maintained to 0 Pa (Figure 4).

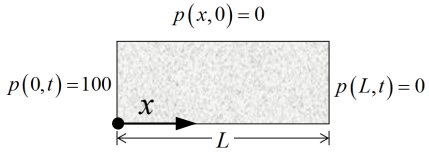

Figure 4. Sample of saturated soil. Initial and boundary conditions.

In order to simplify the model no motion of the solid skeleton has been assumed. The length of saturated soil sample is $L = 1\,\text{m}$ and the bulk modulus of the water is $K_f = 300\,\text{MPa}$. The number of particles considered in the discretization is $Np = 20$ and the total number of nodes is $Nn = 21$ (Figure 5).

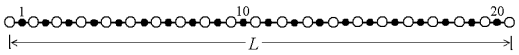

Figure 5. Sample spatial discretization.

The pore pressure distribution along the sample has been simulated. The results have also been compared with the linear steady state solution (Figure 6).

In Figure 6 the dynamic behavior of the problem due to the compressibility of the water is shown. The higher the time is, the better the pressure distribution adjusts the steady state solution. When a gradient of head exists a fluid flow is generated. The analytical expression to calculate the fluid velocity is the well known Darcy's law (Eq.5). For this case the velocity can be written as follows

$$w = -\frac{\mathbf{k}}{\rho_f g}\nabla p \tag{31}$$

where the Darcy's coefficient of permeability is $\mathbf{k} = 10^{-3}$ m/s.

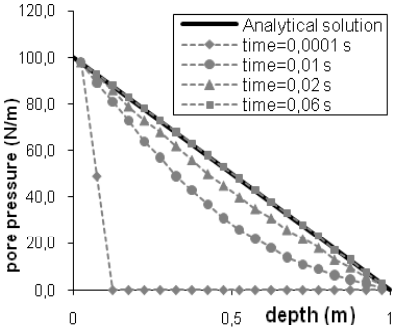

Figure 6. Evolution of the pore pressure along the sample.

The analytical and numerical Darcy's velocities for the particles 1, 10 and 20 (Figure 5) are presented in Figure 7.

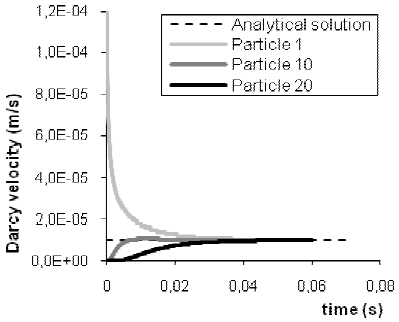

Figure 7. Darcy velocity for particles 1, 10 and 20.

The numerical Darcy velocities for all particles trend to the theoretical result after a short transient period.

CONCLUSIONS

The hydro-mechanical formulation for the MPM has been presented and two problems, one mechanical and another hydraulic, have been modeled. On the basis of the results herein presented the capacity of the model to reproduce the aforementioned examples has been proved. At this point the future goal should be to do further work in order to analyze real coupled problems involving large deformations.

ACKNOWLEDGEMENT

The author acknowledges the grant FPI provided by the Spanish Ministry of Science and Innovation (MICINN), and the support of the Col·legi d'Enginyers de Camins, Canals i Ports de Catalunya. The support and help provided by Pieter Vermeer and Deltares are also thankfully acknowledged.

REFERENCES

[1] D.Sulsky, Z. Chen, & H.L. Schreyer. A particle method for history-dependent materials, *Comput. Methods Appl. Mech. Engng* 118 (1994) 179–196.

[2] D. Sulsky, S.-J. Zhou & H.L. Schreyer. Application of a particle-in-cell method to solid mechanics, *Comput. Phys. Comm.* 87 (1995) 236–252.

[3] D. Sulsky & H.L. Schreyer. Axisymmetric form of the material point method with applications to upsetting and Taylor impact problems, *Comput. Methods Appl. Mech. Engng* 139 (1996) 409–429.

[4] S.G. Bardenhagen, J.U. Brackbill, D. Sulsky, The material-point method for granular materials, *Comput. Methods Appl. Mech. Engrg.* 187 (2000), 529-541.

[5] C.J. Coetzee & P.A. Vermeer, The modeling of anchors using the material point method, *Int. J. Numer. Anal. Methods Geomech.* 29 (2005), 879-895.

[6] F. Zabala & E.E. Alonso. Progressive failure of Aznalcóllar dam using the material point method, Géotechnique. (2010) [doi: 10.1680/geot.9.134].

[7] D.Z. Shang, Q. Zou, W.B. VanderHeyden , Xia Ma. Material point method applied to multiphase flows, *Journal of Computational Physics* 227 (2008), 3158-3173.

[8] O. C. Zienkiewicz, C.T. Chang, P. Bettess. Drained, untrained, consolidating and dynamic behavior assumptions in soils, *Géotechnique* 30, 4 (1980) 385-395.

[9] Z. Wiezckowski, The material point method in large strain engineering problems, *Comput. Methods Appl. Mech. Engrg.* 193 (2004) 4417–4438.

[10] S. G. Baredenhagen. Energy conservation error in the material point method for solid mechanics, *J. of Computational Physics*. 180 (2002) 383-403.